ISSN 1063-7834, Physics of the Solid State, 2009, Vol. 51, No. 9, pp. 1853–1858. © Pleiades Publishing, Ltd., 2009.
Original Russian Text © G.A. Petrakovskiĭ, M.A. Popov, A.D. Balaev, K.A. Sablina, O.A. Bayukov, D.A. Velikanov, A.M. Vorotynov, A.F. Bovina, A.D. Vasil'ev, M. Boehm, 2009, published in Fizika Tverdogo Tela, 2009, Vol. 51, No. 9, pp. 1745–1750.

MAGNETISM AND FERROELECTRICITY

Magnetic Properties of $Pb_2Fe_2Ge_2O_9$ Single Crystals

G. A. Petrakovskiĭ[a, b], M. A. Popov[a, b, †], A. D. Balaev[a], K. A. Sablina[a], O. A. Bayukov[a, b], D. A. Velikanov[a], A. M. Vorotynov[a], A. F. Bovina[a], A. D. Vasil'ev[a, b], and M. Boehm[c]

[a] *Kirensky Institute of Physics, Siberian Branch, Russian Academy of Sciences, Akademgorodok, Krasnoyarsk, 660036 Russia*
e-mail: sasa@iph.krasn.ru

[b] *Siberian Federal University, pr. Svobodnyĭ 79, Krasnoyarsk, 660041 Russia*

[c] *Institut Laue–Langevin, BP 156, rue Jules Horowitz 6, Grenoble Cedex 9, 38042 France*

Received November 24, 2008; in final form, December 16, 2008

Abstract—Single crystals of $Pb_2Fe_2Ge_2O_9$ have been grown. They were subjected to X-ray diffraction, magnetic, neutron diffraction, Mössbauer and spin resonance studies. It has been established that $Pb_2Fe_2Ge_2O_9$ is a weak ferromagnet with a Néel temperature $T_N = 46$ K, and the exchange and spin-flop transition fields have been estimated. It has been demonstrated that the weak ferromagnetic moment is actually the result of the single-ion anisotropy axes for the magnetic moments of different magnetic sublattices being not collinear.

PACS numbers: 75.10.-b, 75.25.+z, 75.30.-m

DOI: 10.1134/S1063783409090145

1. INTRODUCTION

We have studied the magnetic properties of a new compound with chemical formula $Pb_2Fe_2Ge_2O_9$. It is known that compounds whose crystal lattice contains fragments in the form of chains of magnetic atoms display typically remarkable magnetic properties. Belonging to this class are, for instance, $CuGeO_3$, in which Cu^{2+} ion chains undergo dimerization at low temperatures ($T < 14$ K), with the magnetic system transferring to the singlet state by a spin-Peierls phase transition [1]; copper metaborate CuB_2O_4 in which the subsystem of Cu^{2+} chain ions favors transition of the magnetic subsystem to an incommensurate magnetic structure of the type of the soliton lattice [2]; rare-earth ferroborates $REFe_3(BO_3)_4$ with Fe^{3+} chains, which exhibit a pronounced magnetoelectric effect [3]; and chain-structure pyroxenes $AFeGe_2O_6$ (A = K, Na) [4], which hold forth considerable promise as multiferroics [5]. $Pb_2Fe_2Ge_2O_9$ has the structure of the $Pb_2Fe_2Si_2O_9$ melantekite mineral, with zigzag chains of FeO_6 octahedra aligned with the [001] axis of orthorhombic structure [6]. This is what actually prompted our study of this new magnet. $Pb_2Fe_2Ge_2O_9$ attracts also interest by the presence of Pb^{2+} ions in its composition. This ion (6^2s electronic configuration) can be classed among quite rare ions with unbound *s*-electron pairs. Such ions exhibit a high polarizability and tend to assume unusual coordination; in particular, they favor formation of polyhedra lacking inversion symmetry, with the stereochemical ion displaced toward one of the anions of the polyhedron. Crystal structures with such distortions reveal quite frequently remarkable physical characteristics, among them ferroelectric, nonlinear optical and relaxor properties [7, 8].

We report here on the results of magnetic, spin resonance, Mössbauer and neutron diffraction measurements performed on $Pb_2Fe_2Ge_2O_9$ single crystals.

2. GROWTH OF SINGLE CRYSTALS

We grew single crystals of $Pb_2Fe_2Ge_2O_9$. Single crystals of oxide compounds whose composition includes PbO, B_2O_3, Bi_2O_3 and some others used as classic solvents for high-melting compounds can quite frequently be grown from melt solution without addition of other solvents. This method, called melt-pseudo-solution, is known to preclude impurities associated with the solvents employed in single crystal growth from entering the crystal. In choosing the composition of the starting charge and the temperature regime to maintain, we studied the melting diagram of the PbO–GeO_2 system [9], which has several eutectics with temperatures below 740°C. We made use of the method of mass crystallization from the melt solution. A mixture of the PbO (58%), GeO_2 (26%), and Fe_2O_3 (16%) oxides was placed in a platinum crucible, heated to 1050°C, and maintained at this temperature for several hours, followed by cooling at a rate of 2–3°C/h. Prism-shaped dark-brown crystals were up to 4 mm in size and were extracted mechanically out of the crucible. X-ray diffraction analysis performed on powdered crystals on DRON-2 provided supportive evidence for the orthorhombic crystal

† Deceased.

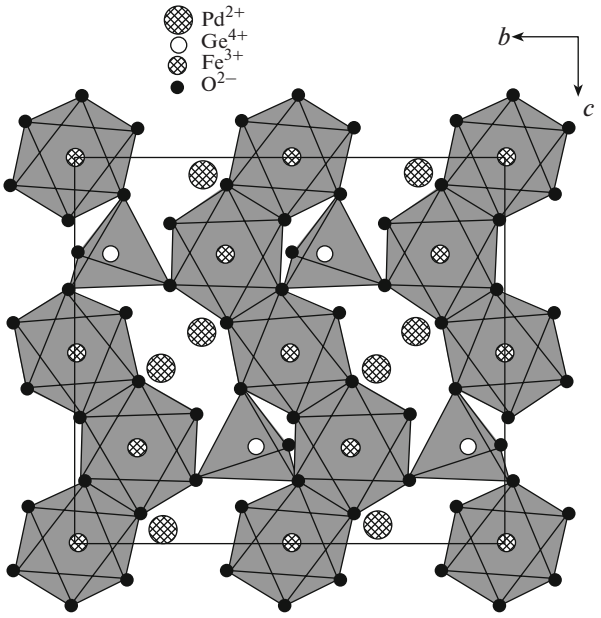

Fig. 1. Projection of $Pb_2Fe_2Ge_2O_9$ structure on the (100) plane.

structure (space group P_{bcn}) with the cell parameters $a = 7.149(3)$ Å, $b = 11.177(4)$ Å, $c = 10.144(3)$ Å, and $z = 4$, in good agreement with the figures reported in [5]. X-ray analysis did not reveal the presence of impurities in noticeable amounts.

3. CRYSTAL STRUCTURE

The crystal structure of the orthorhombic iron germanate $Pb_2Fe_2Ge_2O_9$ was established in [6]. The crystal cell contains four formula units. Figure 1 shows the structure of $Pb_2Fe_2Ge_2O_9$ projected on the (100) plane of orthorhombic lattice. The structure is made up of zigzag chains aligned with the [001] c axis and consisting of edge-sharing FeO_6 octahedra. The chains are linked by tetrahedral Ge_2O_7 germanium groups. Lead ions occupy irregular sites between the chains. There are two inequivalent octahedral positions for the Fe^{3+} ions, Fe1 (4*a*) and Fe2 (4*c*). These positions, alternating along the chains, differ slightly in the degree of distortion of the oxygen coordination octahedron and

Parameters of room-temperature Mössbauer spectrum of $Pb_2Fe_2Ge_2O_9$

Position	IS	QS	W	S
4*a*	0.38	1.11	0.31	0.49
4*c*	0.39	1.37	0.30	0.51

Note: IS is the isomer shift relative to α-Fe (±0.02 mm/s), QS is the quadrupole splitting (±0.02 mm/s), W is the absorption line FWHM (±0.03 mm/s), and S is the fraction of the position population (±0.03 mm/s).

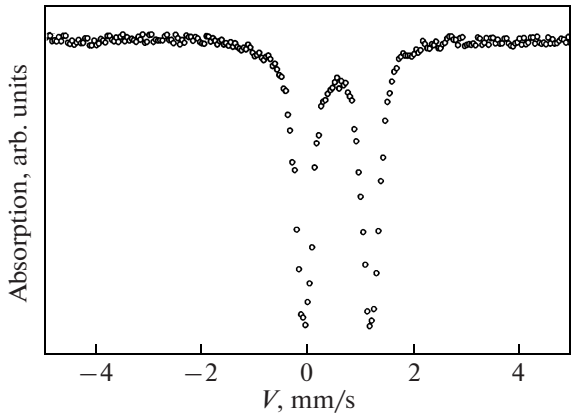

Fig. 2. Room-temperature Mössbauer spectrum of $Pb_2Fe_2Ge_2O_9$.

second-neighbor environment symmetry. The oxygen octahedra are contracted for both positions. Defining the degree of octahedron distortion by the difference in length between the major and minor octahedron axes, we can say that the Fe2 position is more strongly distorted. Our Mössbauer study supports this statement. The Mössbauer spectrum was measured at room temperature on a powder sample prepared by grinding the crystals. The pattern of the spectrum (Fig. 2) reflects the insignificant difference in the degree of oxygen octahedron distortion and electron density at the core between the two inequivalent Fe^{3+} ion positions.

The Fe1–O–Fe2 distance in the chain ~4 Å is the shortest; hence, it appears reasonable to assume that the exchange interaction between Fe^{3+} ions is maximal along the chain. The interchain coupling occurs through Fe–O–Pb–O–Fe and Fe–O–Ge–O–Fe bridges ~8.5 Å long and is apparently substantially weaker than the intrachain coupling.

4. MAGNETIC MEASUREMENTS

The static magnetic properties of $Pb_2Fe_2Ge_2O_9$ single crystals were measured on a computerized vibrating-sample magnetometer with a superconducting coil within a temperature range of 4.2–300 K and in magnetic fields of up to 75 kOe. The prism-shaped sample measuring 0.4 × 0.6 × 3 mm with a rhombic base was oriented visually in accordance with its faceting, and the larger size of the prism was aligned with the c axis. The measurements were performed with the magnetic field $H = 1$ kOe oriented along the three mutually perpendicular directions. We studied the temperature and field dependences of magnetic susceptibility in the paramagnetic and magnetically ordered phases. The results of the measurements are displayed graphically in Fig. 3.

We immediately see a clearly pronounced anisotropy in the temperature dependences of magnetic sus-

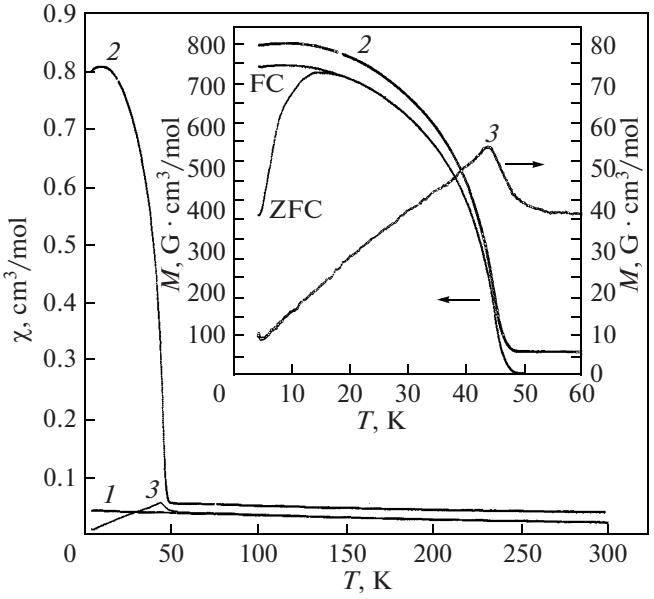

Fig. 3. Temperature dependence of the susceptibility of $Pb_2Fe_2Ge_2O_9$ in a field $H = 1$ kOe: (*1*) $\mathbf{H} \parallel a$, (*2*) $\mathbf{H} \parallel b$, and (*3*) $\mathbf{H} \parallel c$. The inset shows the magnetization of the sample on an enlarged scale. The magnetization $\mathbf{H} \parallel b$ is plotted for different cooling conditions (ZFC is the zero-field cooling, and FC is the cooling in an external field).

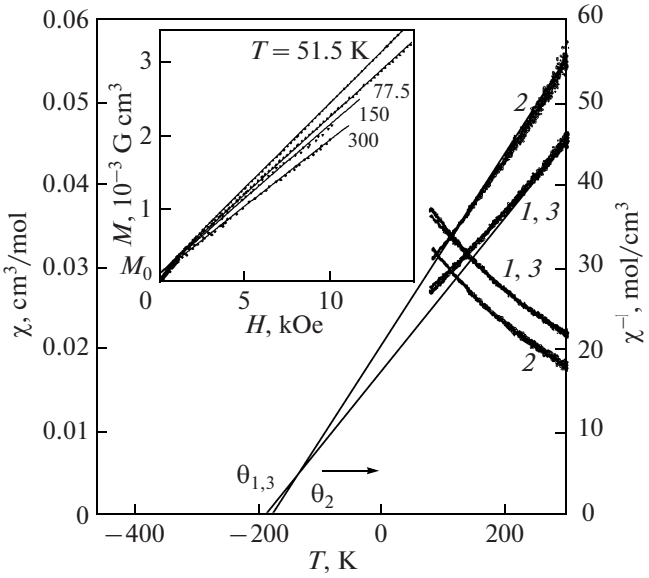

Fig. 4. Temperature dependences of forward and reverse magnetization of $Pb_2Fe_2Ge_2O_9$ plotted for different external magnetic field orientations. The curve notation is the same as in Fig. 3. The inset shows the temperature-independent contribution ($M_0 = \chi_0 H$) along the crystal *b* axis.

ceptibility and a transition to a magnetically ordered state at $T_N = 46$ K. For a magnetic field parallel to the *b* axis, a weak ferromagnetic moment is seen to appear below 46 K, which grows rapidly with decreasing temperature. In this direction, the magnetization was found to depend on the measurement regime used, more specifically, the zero magnetic field and field cooling. The low-field magnetization measurements performed with the magnetic field aligned with the *b* axis at different temperatures below 46 K revealed the presence of hysteresis loops. The coercive field at low temperatures is about $H_c \sim 300$–400 Oe and decreases with increasing temperature. The effect of external field on the temperature dependence of magnetization is probably connected with magnetic moments at domain boundaries being blocked. The blocking temperature depends on external magnetic field.

The temperature dependence of the susceptibility $\chi_c(T)$ measured in a field of 1 kOe (Fig. 3), which was applied along the *c* axis, reveals a sharp peak near T_N, a feature characteristic of a field directed along the antiferromagnetic axis ($\chi_\parallel$). The susceptibility $\chi_\perp$ measured along the *a* axis practically does not depend on temperature and has no anomaly near T_N. Thus, there is an anisotropy in susceptibility, $\chi_\parallel$ and $\chi_\perp$, in the *ac* plane perpendicular to the *b* axis (and the weak ferromagnetic moment).

Above T_N, the susceptibility was measured both on a set of crystallites and on one single crystal with different magnetic field orientations relative to the crystal axes. From the linear part of the $\chi^{-1}(T)$ relation, within which the Curie–Weiss law holds, we determined the Curie–Weiss temperature $\Theta = -160$ K and $\mu_{eff} = 6.03\ \mu B$. The negative sign of the Curie–Weiss temperature suggests that antiferromagnetic exchange interactions dominate in the crystal and that μ_{eff} is close to the theoretical value for the Fe^{3+} ion, $\mu_{eff}^{theor}(Fe^{3+}) = 5.92\ \mu_B$.

Similar measurements performed on the single crystal (Fig. 4) showed that the $\chi^{-1}(T)$ relations measured with the field directed along the *a* and *c* axes practically coincide, with $\Theta = -180$ K and $\mu_{eff} = 6.4\ \mu_B$. The $\chi_b(T)$ curve has a temperature-independent constant, $\chi_0 \cong 2.1 \times 10^{-2}$ cm³/mol, with $\Theta_b = -170$ K, $\mu_{eff} = 5.9\ \mu_B$ after its subtraction.

The field dependences of magnetization behave differently along different crystal axes. Measured in a magnetic field oriented along the *a* axis in the temperature interval of 4.2–77.5 K, they plot practically as straight lines up to fields of 75 kOe with the slope decreasing with increasing temperature. The *a* direction is obviously perpendicular both to the antiferromagnetic axis and the direction of the weak ferromagnetic moment.

Figure 5 displays magnetization isotherms with the magnetic field along the *b* axis. Within the 4.2–45-K interval, the magnetization may be considered as a

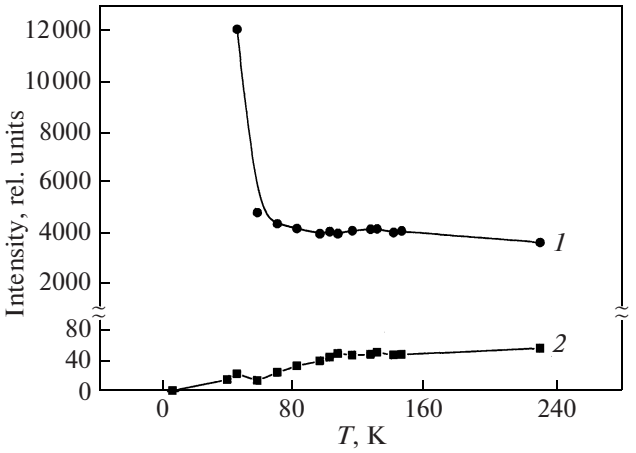

Fig. 9. Behavior with temperature of the intensities of signals *1* and *2* in $Pb_2Fe_2Ge_2O_9$.

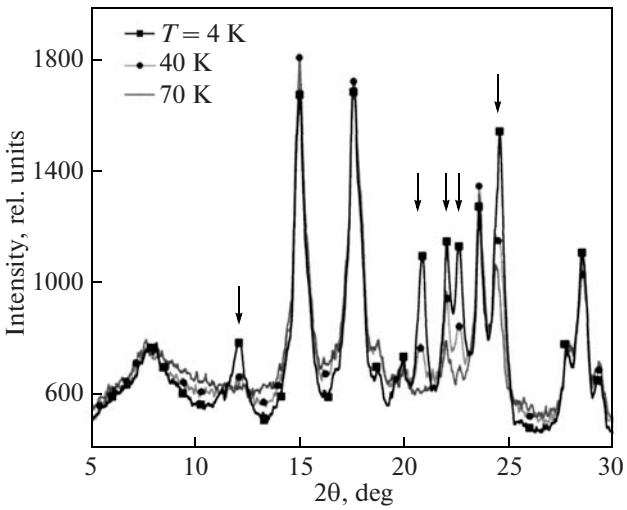

Fig. 10. X-ray powder diffraction pattern of $Pb_2Fe_2Ge_2O_9$ obtained at small scattering angles and at different temperatures. The magnetic peaks are identified by arrows.

scopic splitting factor). For Fe^{3+}, $J = S = 5/2$, $2H_{ea} = 1504$ kOe, $2H_{eb} = 1473$ kOe, and $2H_{ec} = 1427$ kOe.

5. ESR SPECTRA

The ESR spectra were measured with a Brucker *X*-range spectrometer at temperatures of 4.2–300 K and different magnetic field orientations relative to the crystal axes. A typical spin resonance spectrum is shown in Fig. 7.

The spectrum consists of two lines labeled *1* and *2*: a broad line with the parameters $g_\perp = 2.045$, $g_\parallel = 2.003$, $\Delta H_\perp = 2313$ Oe, and $\Delta H_\parallel = 2700$ Oe and a narrow line with the parameters $g_\perp = 2.208$, $g_\parallel = 2.194$, $\Delta H_\perp = 410$ Oe, and $\Delta H_\parallel = 410$ Oe at room temperature.

The behavior with temperature of the linewidths and *g* factors is plotted in Fig. 8. The linewidth of signal *1* increases monotonically with decreasing temperature. The line broadens critically as one approaches the Néel temperature $T_N = 46$ K to disappear altogether. The *g* factor varies at low temperatures to $g_\perp \approx 5$, and the line shifts to the weak field domain.

The linewidth of signal *2* is practically temperature independent, and the value of the *g* factor grows monotonically within the 50–100-K interval. Below $T = 50$ K, the *g* factor decreases to reach $g = 2.85$ at helium temperatures.

Figure 9 compares the intensities of lines *1* and *2* defined as products of the signal amplitude by the square of linewidth. We note that the intensity of signal *2* is weaker by several orders of magnitude than the intensity of signal *1* and that it decreases with decreasing temperature.

6. NEUTRON DIFFRACTION STUDIES

To verify the presence of long-range magnetic order in $Pb_2Fe_2Ge_2O_9$, we studied elastic neutron scattering. The study was performed with the use of a high-resolution *D2B* powder diffractometer (l'Institut Laue-Langevin, Grenoble, France) operating at a wavelength $\lambda = 1.49$ Å. The powder spectra were measured at several temperatures below the magnetic ordering point T_N and at 70 K, i.e., above the transition temperature. An analysis of these spectra made invoking the corresponding crystallographic data [6] demonstrated a good agreement of the experimental with calculated neutron scattering spectra and permitted assignment of the magnetic peaks appearing at temperatures below $T_N = 46$ K. Figure 10 presents a part of the diffractogram obtained at small scattering angles. The arrows identify the magnetic peaks that appeared at temperatures below 46 K and whose intensity grows continuously to $T = 4.2$ K.

One observes also quite pronounced diffuse scattering of neutrons at small scattering angles and a temperature $T = 70$ K, whose intensity falls off with decreasing temperature in the proportion in which that of the magnetic Bragg reflections increases. It may suggest that this diffuse scattering is of magnetic origin and, thus, signals the onset of short-range magnetic order above the magnetic phase transition temperature.

These neutron diffraction data show convincingly that $Pb_2Fe_2Ge_2O_9$ has a complicated antiferromagnetic structure. Identification of its exact pattern requires additional measurements on a crystal sample.

7. DISCUSSION

An analysis of the totality of experimental data amassed in magnetic and neutron diffraction studies permits a conclusion that $Pb_2Fe_2Ge_2O_9$ is a weak ferromagnet with an antiferromagnetic axis directed along the crystal *c* axis and a weak ferromagnetic moment aligned with the *b* axis. The weak ferromagnetic moment is strongly anisotropic and manifests itself only along the *b* axis. It is known that it is such a strong anisotropy in the magnetic properties of a weak ferromagnet that is the signature of weak ferromagnets with rhombohedral crystal structure [10]. The weak ferromagnetism is observed actually only along one ("easiest") direction (the *b* axis in our case), while along the other two axes, the crystal behaves as a conventional antiferromagnet. Considered in the frame of the simplest two-sublattice model, a weak ferromagnetic moment is described by an invariant of single-ion anisotropy of the kind

$$M_{1x}M_{1y} - M_{2x}M_{2y}. \quad (1)$$

In this context, the magnetization process is qualitatively described by the thermodynamic potential of a rhombohedral crystal [10]

$$\Phi = (1/2)Jm^2 + (1/2)(K_a l_x^2 + K_c l_z^2) + d(l_x m_y + l_y m_x) - \mathbf{mh}, \quad (2)$$

where **m** and **l** are, accordingly, ferro- and antiferromagnetic vectors; *J* is the exchange interaction parameter; K_a and K_c are the constants of anisotropy along the corresponding crystal axes; *d* is the parameter of single-ion anisotropy of weak ferromagnetic interaction; and **h** is the external magnetic field. For the spin-flop transition field we have

$$H_{sf} = [J(K_c - K_a)]^{1/2}. \quad (3)$$

Assessments of the sublattice canting angle α and the exchange and anisotropy fields yield the following estimates ($M_0 = ngS\mu_B$, *n* is the number of formula units per cell):

$$\sin\alpha = H_d/2H_e, \quad \alpha = 0.8°,$$

$$H_e = J/4M_0 = 1400 \text{ kOe}, \quad H_d = d/2M_0 = 21 \text{ kOe}.$$

Estimation of intrachain exchange interaction gives $J_1 \sim 5$ K. Three-dimensional antiferromagnetism is generated by interchain exchange interactions J_2 over the Fe–O–Pb–O–Fe and Fe–O–Ge–O–Fe extended indirect bonds, and, therefore, $|J_2| \ll |J_1|$. ESR measurements provide supportive evidence for the magnetism of this compound being mediated by Fe^{3+} ions with the *g* factors $g_\perp = 2.208$ and $g_\parallel = 2.194$. The temperature-independent ESR line should apparently be assigned to a residual impurity.

8. CONCLUSIONS

The $Pb_2Fe_2Ge_2O_9$ compound is a weak chain orthorhombic ferromagnet with an ordering temperature of 46 K. The weak ferromagnetic moment is due essentially to the axes of single-ion anisotropies for the magnetic moments belonging to different magnetic sublattices being noncollinear. It is directed only along the *b* axis of the crystal. In a magnetic field oriented along this axis, one observes a spin-flop transition with a critical field $H_{sf} \sim 50$ kOe. Neutron diffraction measurements corroborate the onset of long-range antiferromagnetic order at $T < T_N = 46$ K. To establish a detailed pattern of the magnetic order, which neutron diffraction measurements suggest to be far from trivial, additional neutron diffraction studies would be needed.

REFERENCES

1. G. Petrakovskii, in *Itinerant Electron Magnetism* Ed. by D. Wagner, W. Brauneck, and A. Solontsov (Kluwer, Dordrecht, The Netherlands, 1998), p. 437.
2. B. Roessli, J. Schefer, G. Petrakovskii, B. Ouladdiaf, M. Boehm, U. Staub, A. Vorotinov, and L. Bezmaternikh, Phys. Rev. Lett. **86**, 1885 (2000).
3. A. K. Zvezdin, G. P. Vorob'ev, A. M. Kadomtseva, Yu. F. Popov, A. P. Pyatakov, L. N. Bezmaternykh, A. V. Kuvardin, and E. A. Popova, Pis'ma Zh. Éksp. Teor. Fiz. **83** (11), 600 (2006) [JETP Lett. **83** (11), 509 (2006)].
4. T. V. Drokina, O. A. Bayukov, G. A. Petrakovskiĭ, D. A. Velikanov, A. F. Bovina, G. N. Stepanov, and D. A. Ivanov, Fiz. Tverd. Tela (St. Petersburg) **50** (11), 2050 (2008) [Phys. Solid State **50** (11), 2141 (2008)].
5. S. Jodlauk, P. Becker, J. Mydosh, J. Khomskii, D. Lorenz, S. Streltsov, D. Hezel, and L. Bohaty, J. Phys.: Condens. Matter. **19**, 432201 (2007).
6. J. Barbier and D. Levy, Acta Crystallogr., Sect C: Cryst. Struct. Commun. **54**, 2 (1998).
7. D. I. Khomskii, J. Magn. Magn. Mater. **306**, 1 (2006).
8. S. Ivanov, R. Tellgren, H. Rundlof, N. Thomas, and S. Ananta, J. Phys.: Condens. Matter **12**, 2393 (2000).
9. N. A. Toropov, V. P. Barzakovskiĭ, V. V. Lopatin, and N. N. Kurtseva, *Phase Diagrams of Silicate Systems* (Nauka, Moscow, 1965) [in Russian].
10. E. A. Turov, A. V. Kolchanov, V. V. Men'shenin, I. F. Mirsaev, and V. V. Nikolaev, *Symmetry and the Physical Properties of Antiferromagnets* (Fizmatlit, Moscow, 2001) [in Russian].

Translated by G. Skrebtsov